

EXCAVATION EFFICIENCIES IN THREE-DIMENSIONAL SIMULATIONS OF THE CHICXULUB METEOR IMPACT

G. R. Gisler⁽¹⁾, R. P. Weaver⁽²⁾, M. L. Gittings⁽³⁾

⁽¹⁾*Physics of Geological Processes, University of Oslo, PO Box 1048 Blindern, 0316 Oslo, NORWAY
Email: galen.gisler@fys.uio.no*

⁽²⁾*Los Alamos National Laboratory, MS T087, Los Alamos, NM 87545 USA, Email: rpw@lanl.gov*

⁽³⁾*Science Applications International, MS T087, Los Alamos NM 87545 USA, Email: gittings@lanl.gov*

ABSTRACT

Simulations of the meteor impact at Chicxulub with the Los Alamos hydrocode SAGE are presented here for four angles of impact. We describe the code and its validation, including a comparison of simulation results with measurements at the crater from the Sedan underground nuclear test. We investigate energy partitioning and excavation efficiency as a function of impact angle, and discuss implications for the consequent distribution of ejected material. We find that the impact angle must be fairly steep to account for the worldwide distribution of shocked quartz.

1. INTRODUCTION

We have performed several three-dimensional simulations of the meteor impact at Chicxulub, Mexico with the Continuous Adaptive Mesh Refinement Eulerian hydrocode SAGE. The Chicxulub impact, which occurred 65 million years ago, is widely believed to be associated with the mass-extinction event at the end of the Cretaceous period and may have caused this extinction by a combination of widespread wildfires, high atmospheric opacity, atmospheric toxicity, and severe climate excursions. The worldwide distribution of shocked quartz, platinum-group elements, tektites, and soot in the Cretaceous/Tertiary (K/T) boundary layer can provide important diagnostics of the dynamics of the impact and the mechanisms of extinction [1]. Studies of the energy partitions and excavation efficiencies among simulations at various angles of impact and projectile characteristics are useful in elucidating the relation between the impact event, the distributed evidence in the K/T boundary layer, and the extinction mechanism.

2. SAGE

The SAGE code is a fully-compressible multiphase multifluid hydrocode using a Godunov scheme for second-order accuracy. It has been jointly developed by the Los Alamos National Laboratory and Science

Applications International (SAI). Developed under the auspices of the Department of Energy's program in Advanced Simulation and Computing, it has been exposed throughout its development to very rigorous testing against problems with analytical solutions, for verification. See for example [2], which reports the results of a recent series of these tests and describes an automated scheme for continued testing of new versions of the code in the same manner. Validation, or testing against controlled laboratory-scale experiments is also done according to a timetable [3]. SAGE has additionally been applied to large-scale geophysical events including volcanic eruptions and tsunamis [4], where neither control nor precision testing is possible. In these cases we aim for consistency with the *a posteriori* geophysical data, and achieve this.

Because the equations of hydrodynamics are not in themselves closed, additional information regarding the response of materials to stress must be supplied. These are in the form of equations of state (for isotropic stresses) and constitutive relations, which relate the stress tensor and the internal energy to local densities and temperatures. In practice, these relations are known to be the weakest part of complex multi-fluid hydrocode simulations, because the codes often explore regimes in phase space that are not well covered by the laboratory experimentation that is used to derive these relations. SAGE includes a variety of analytical formulations of these equations of state and constitutive relations, but these are inadequate for complex geophysical use. Better are the equation of state and strength tables from the Los Alamos SESAME library, which unfortunately does not have good coverage of geological material. What exists in SESAME is mostly derived from light gas gun experiments carried out decades ago and extended to regions off the Hugoniot by theory. In the Chicxulub simulations we use SESAME tables for air, calcite, granite, and mantle material. We find, however, that we must modify the output from the SESAME tables to enforce thermodynamic consistency (including the latent heats of phase transitions, removing the van-der-Waals loops, etc). In addition, SAGE contains a special tabular equation for water designed by SAI to include nearly all known phase transitions.

It is important to realize that in a multimaterial Eulerian code like SAGE, some decision must be made as to how to treat cells that receive a mixture of materials.

There are interface treatments available within SAGE that allow one to keep track of the position of an interface on a sub-grid scale if desired. Such treatments allow one to inhibit or limit mixing, if so desired. We have not used any such interface treatment in these calculations. The default method, which we have used, is to assume that within each Eulerian cell local thermodynamic equilibrium obtains among the materials that occupy that cell. Because the adaptive grid mechanism ensures that adaption occurs to the maximum extent allowed by the user at a material interface, the equilibration that occurs within a single timestep occurs on the smallest cells in the problem. The equilibration is made thermodynamically consistent, ensuring conservation of total energy.

For materials in the problem that have strength, a simple elastic-perfectly plastic strength model is used, with pressure hardening, tensile failure, and melt energy. On impact, the transition from solid to liquid (indeed to vapor for much of the immediate target) is so rapid that the details scarcely matter, provided the latent heat of transition, the induced pressure, and the consequent volume change are properly accounted for. No specific fragmentation model was used in these calculations.

Because the material models are such an important part of the computational enterprise for a problem such as Chicxulub, it is important to have some validation, or at least benchmarking, experience with events at comparable scale that utilize the same material models. Realistically, the only geophysical events that even approach the scale of planetary impact craters while having known inputs of energy are underground nuclear explosions. We take in particular the Sedan nuclear test of July 1962, done for the Plowshare program, and intended to investigate possible peaceful uses of nuclear explosions. The Sedan device was buried 194 m below the surface of the Nevada test site desert and exploded with an energy of 104 kT. The emplacement depth was close to the optimum depth for cratering, and the resultant crater is a good test for cratering simulations. Fig. 1 shows the result of a comparison between a SAGE calculation (colors indicating material density) of the crater resulting from Sedan, still at an early stage, before fallback has completed, and measurements taken at the crater itself (the solid lines). The agreement is remarkably good. The crater diameter of 360 m, the maximum melt depth of 246 m, and the final crater depth of 97 m are well matched by the calculation (only the melt depth being somewhat overestimated). The maximum height of the dome before its breach, 90 m, and the time of the dome breach, 3 seconds after initiation, are also reasonably well matched by the calculation.

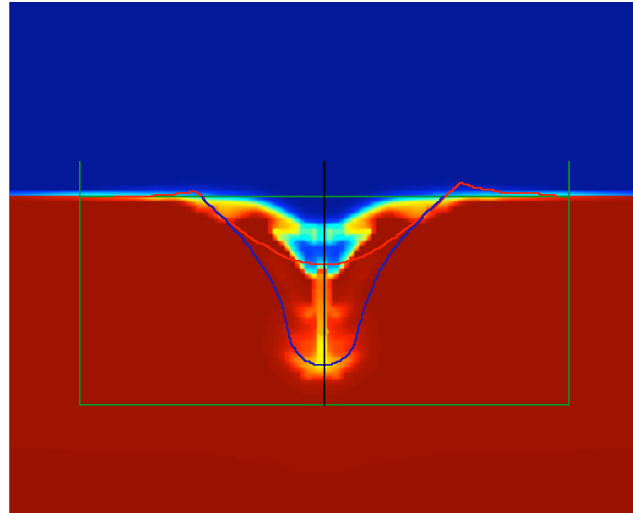


Fig. 1. Comparison between a SAGE calculation (colors representing density), and measurements taken on site of the Sedan underground nuclear explosion. The red solid line indicates the shape and size of the final crater, and the blue solid line indicates the extent of the below-ground melt.

3. SETUP FOR THE CHICXULUB SIMULATIONS

All simulations reported here were performed in a computational domain which is a box with horizontal dimension 256 km x 256 km and vertical dimension 128 km. The target consists of a US standard atmosphere of scale height 7 km, extending up to an altitude of 78 km, a water depth of 500 meters, a mixed water/solid calcite region 4.5 km thick, linearly stratified from pure water at the top to pure calcite at the bottom, a granite region 30 km thick, and a mantle region 15 km thick. This vertical stratification is illustrated schematically in Fig. 4 below. The target is homogeneous in the horizontal directions.

The projectile in the runs reported here is a sphere of 12 km diameter, with the density and equation of state of granite, but without strength, and having a velocity of 20 km/s. The total kinetic energy is therefore 113 Tt. An earlier series of runs performed with an earlier version of SAGE with a slower and lighter projectile is mentioned here only in passing. The 4 runs here reported have projectile trajectories of 15°, 30°, 45° and 60° with respect to the horizontal. All projectiles were started at an altitude of 40 km, except for the 15° run, in which a 20 km initial altitude was used. Outflow boundary conditions (freeze regions) are used.

We run these simulations until most of the ejected material has either achieved ballistic trajectories or been deposited locally. This generally requires two to three minutes of physical time, or several months of computational time on 512 processors. So far we have achieved this with all but the 60° simulation, which has only run out to 17 seconds past impact. These longer-time studies supplement earlier work by Pierazzo and

collaborators on effects of impact angle [5].

4. RESULTS

The only free energy at the start of the problem is the asteroid's kinetic energy. Upon impact, this energy is shared with the target, which responds both by being accelerated out of the way and by heating up. In Fig. 2 we plot the partition of kinetic and internal energies as a function of impact angle for the projectile and target at 5 seconds after the asteroid's kinetic energy is reduced to 75% of its initial value. The lines indicating internal energy represent the changes from initial values of internal energy, of course. As is expected, shallow impacts deliver much less energy to the target than deep impacts do. For very shallow impacts, much of the energy is retained in the form of the asteroid's kinetic energy, whose material propagates downrange on flattened "skipping" trajectories to impact again downrange.

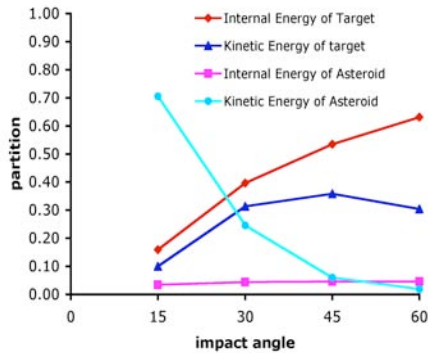


Fig. 2: Partition of energies (relative to the initial asteroid kinetic energy) at 5 seconds after the time at which the projectile's kinetic energy is 75% of its initial value for the 4 runs reported here. At shallow angles of impact, most of the initial kinetic energy is retained by the asteroid, whose material skips downrange in a relatively tightly focussed stream. At angles of impact greater than about 45°, more than 90% of the energy of impact is transmitted to relatively deeply excavated target material.

Because impacts at shallow angles deliver much less energy to the target, they also do not excavate very deeply. The worldwide distribution of ejected material suggests that significantly deep excavation has taken place in this event. In particular, shocked quartz, which is produced by the rapid application of high pressure to granite, is found in the K/T boundary layer at places very far distant from Chicxulub [6]. Since the granite of the continental crust at Chicxulub lies buried beneath several kilometers of carbonate platform, it is clear that deep excavation must be relatively efficient to account for the worldwide distribution of shocked quartz.

We diagnose excavation efficiencies by studying the trajectories and histories of Lagrangian tracer particles that are placed at particular positions at the beginning of the calculation. These tracers are massless points that move with the local flow and record as many local variables as desired. Typically we record pressure, temperature, density, and the three components of velocity. Unfortunately the treatment of tracers in SAGE has been rather clumsy and inefficient (the tracer data is written out in text format from a single processor, for example), so that it is deleterious to the parallel performance of the code to follow more than a few hundred such tracers in a given calculation.

In these calculations we have sprinkled a total of 213 tracers, 69 of them in the projectile and the remainder around the impact site down to mantle depths. Each target tracer originates within a given target layer, but it may later reflect the characteristics of a different material, or a mixture of materials. If a tracer that began in a one-material cell ever lands in an Eulerian cell that is a mixed cell, it will adopt the local variables of that cell, which is of course a mixture. Because of this change in the material that a tracer might represent, for more reliable statistics it would obviously be much more desirable to have hundreds of tracers for every one that we have used in these simulations, and improvements in SAGE will make it possible to do so in the future.

Nevertheless, with the limited tracer data that we have, we can make some generalizations about the relative excavation efficiencies of shallow versus steep impact angles. Shallow angle impacts simply do not excavate enough granite to account for the distribution of shocked quartz from the Chicxulub event. In fact, at an angle as low as 15°, most of the energy of impact is retained in the fragmented and vaporized asteroid material, which mainly propagates downrange at relatively low altitude (Fig. 3).

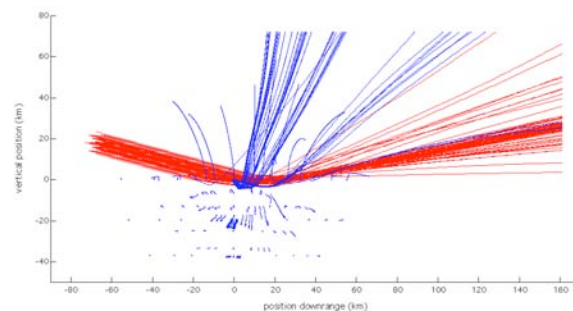


Fig. 3: X-Y projection of tracer particle trajectories out to 120 seconds for projectile (red) and target (blue) tracers for the 15° run. Excavation of target material is very shallow, very little projectile material is deposited in the crater, and the projectile remains are strongly focussed downrange.

At successively greater angles of impact (Figs. 4 and

5) more granite is excavated, and with more energy and greater isotropy. The dispersal of projectile material also becomes more uniform with steeper angles of impact. These results suggest that a relatively steep angle of impact (45° or greater) may be necessary to account for the worldwide distribution of platinum-group elements in the K/T boundary layer and also for the similarly broad distribution of shocked quartz [7]. We do not yet have similar results for our 60° run, as it is still in progress at this writing, but what we have seen so far is consistent with the arguments we make here.

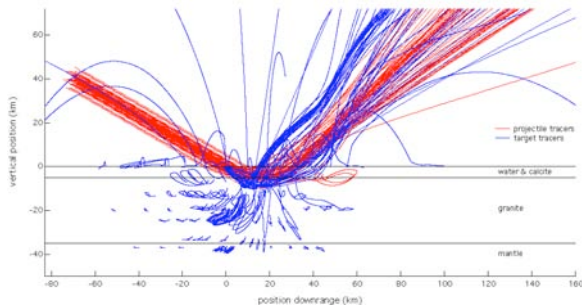


Fig. 4: X-Y projection of tracer particle trajectories out to 240 seconds for projectile (red) and target (blue) tracers for the 30° run. There is more spreading of both target and projectile material than in the 15° run, and some projectile tracers end up buried within the crater. The vertical stratification in the graph indicated here is the same in all model runs.

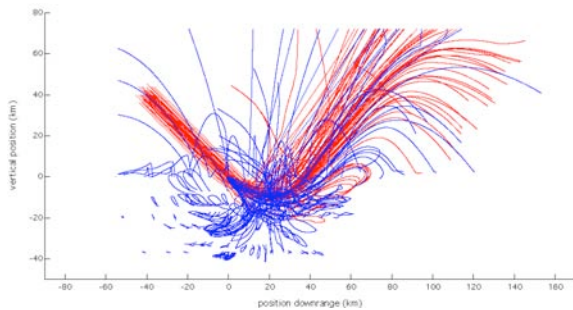


Fig. 5: X-Y projection of tracer particle trajectories out to 160 seconds for projectile (red) and target (blue) tracers for the 45° run. The ejection of target tracers is more symmetric than in the shallower runs, and a larger proportion of them achieve injection into the stratosphere or into suborbital ballistic trajectories. Still more projectile material is buried within the crater, and more rains back locally than in the shallower impact runs.

Similar conclusions can of course be derived from consideration of the peak pressures achieved in impacts at different angles. Of particular interest for excavation efficiency is the peak pressure at the calcite/granite interface which is shown as a function of angle in Fig. 6.

We see once again that the steeper impact angles are much more likely to result in greater distribution of shocked quartz than impacts at shallow angles.

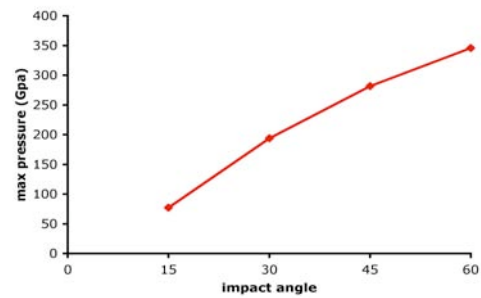


Fig. 6: Peak pressures seen at the calcite-granite interface for the 4 runs reported here, presented as a function of the impact angle.

An estimate of the actual amount of target material that is excavated and ejected into the stratosphere can be obtained by examining the trajectories of the tracers that originated within those materials of the target, and for those tracers that have achieved ballistic trajectories, extending them to their apogees. Each tracer is then taken as representing some volume of the material it originated within, and if this tracer has an apogee greater than stratospheric altitude the volume associated with it is regarded as deposited into the stratosphere. Fig. 7 illustrates the stratospheric input from the asteroid and three components of the target.

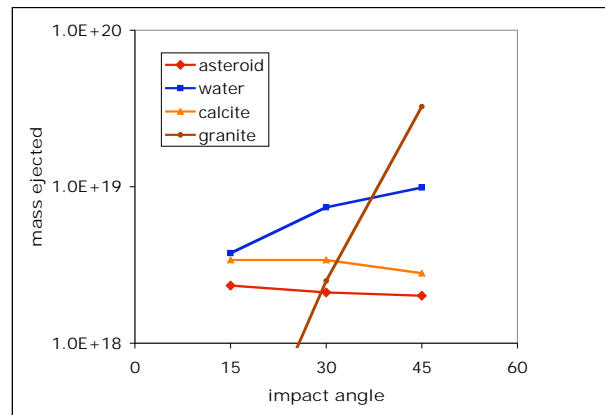


Fig. 7: Mass deposited into the stratosphere for four materials in the problem as functions of the impact angle.

While mass deposition into the stratosphere is perhaps the most significant influence of the Chicxulub impact event upon the environment in the late Cretaceous, another factor to be considered is the direct input of thermal energy into the troposphere via the atmospheric shocks that are produced during the course of the impact itself and the explosive vaporization of volatile materials that subsequently ensues. The atmospheric shocks are asymmetric. First there is the shock that is produced

surrounding the trajectory of the meteor in its passage through the atmosphere. Following passage of the shock, a hot and rarefied medium persists uprange of the asteroid for some minutes. If the trajectory is flat (shallow impact angle), this low-density channel is inaccessible to most of the heated material produced in the second shock, due to the excavation and explosive vaporization of the target. Instead, the horizontal component of the asteroid's momentum causes entrainment of the vaporized target material in the downrange direction. This effect may be seen in Figs. 3 and 4. Much of this very hot material is injected forcefully into the troposphere and could cause ignition of vegetation at considerable distance downrange, as well as effecting a serious and potentially devastating, but undoubtedly temporary, disruption to global atmospheric circulation patterns.

On the other hand, if the trajectory is steep, the rarefied channel produced by the incoming projectile is high in the atmosphere and therefore remains accessible to some of the rising material from the explosive vaporization of the target. The horizontal component of the asteroid's momentum is less, and there is consequently less entrainment of heated material in the downrange direction (see Fig. 5), and the entrainment that does occur is at higher altitude than in the flat case, providing less direct thermal input into the troposphere.

Thus more thermal energy is injected directly into the troposphere downrange of the impact point for shallow-angle impacts, while considerable thermal energy can escape through the top of the atmosphere when the impact angle is steep. In a shallow-angle impact, it would therefore be expected that fires would be immediately ignited on land downrange from the impact site, while for a steep-angle impact the first fires might well be set at points very distant from the impact site, even near the antipode, by the hot re-entry of ballistically ejected material. The lack of charcoal deposits in K/T boundary sediments in North American sites [8] might be seen as providing an additional argument that the impact angle must not have been shallow. On the other hand, the lack of charcoal could, and probably does, indicate much more complete combustion.

Summing up these considerations, we conclude that a shallow angle of impact might have resulted in an extinction mechanism involving the direct injection of thermal energy into the local troposphere, causing extensive local fires and strong hot winds. A steeper angle would be more likely to affect the global stratosphere within the first two hours, poisoning and darkening the atmosphere worldwide and heating via ballistic re-entry of asteroidal and target material. Signatures of these two distinct mechanisms would seem to be quite different, and the distribution of shocked quartz and tektites in very distant locations tends to support the steeper angle hypothesis.

Of course it is also the case that a shallower angle of impact will produce a smaller crater, so that a fair comparison of the amount of material ejected must be made with simulations that all produce a crater the size

of Chicxulub, which means that the simulations for shallower angles must be made with larger or faster projectiles, or both. We have not done this; we kept the same projectile diameter and speed for all four runs. We note, however, that the quantity of granite ejected into the stratosphere differs by *orders of magnitude* among the three runs plotted in Fig. 7, while the crater diameter (Fig. 8) differs by only ~30% among the same three runs.

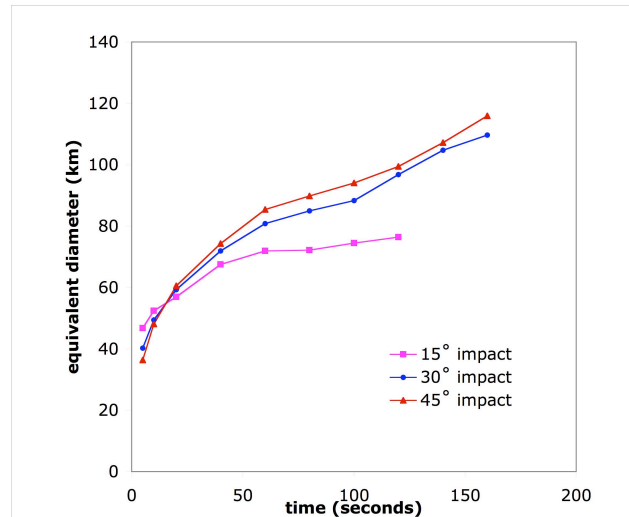


Fig. 8: Crater diameters as a function of time for the three runs that have gone out beyond 20 seconds. These diameters are defined by taking the position of the first zero-crossing of the density=1 isosurface averaged over all directions from the impact center, and may be taken as representing the early transient crater evolution. The transient crater diameter at Chicxulub is in dispute, but is at any rate not much greater than the numbers reported here.

We therefore consider our result on excavation efficiency robust, although our future simulations of this event will adjust the energies accordingly, and also make use of better tracer handling and other improvements to the SAGE code.

5. REFERENCES

1. Smits J. *Ann. Rev. Earth Planet. Sci.* 27:75-113, 1999.
2. Timmes F., Gisler G., Hrbek G., Los Alamos Unclassified Report LA-UR 05-6865, 2005.
3. Zoldi C., Los Alamos Unclassified Report LA-UR 02-6600, 2002.
4. Mader C. L. & Gittings M. L., "Modeling the 1958 Lituya Bay mega tsunami, II", *Science of Tsunami Hazards*, **20**, 241, 2002.
5. Pierazzo E. and Melosh H. J. *Ann. Rev. Earth Planet. Sci.* 28:141-67, 2000.
6. Claeys P., Kiessling W., Alvarez W., *Geological Society*

of America Special Paper 356, 55-68, 2002

7. Crookell M. et al. *Geophys. Res. Lett.*, 29, No. 20, 2002.

8. Belcher C. M. et al. *J. Geol. Soc. Lond.* 162, 591-602, 2005.